Acta Mech 226, 2497–2510 (2015)
DOI 10.1007/s00707-015-1330-6

ORIGINAL PAPER

M. Abdollahi · A. R. Saidi · M. Mohammadi

Buckling analysis of thick functionally graded piezoelectric plates based on the higher-order shear and normal deformable theory

Received: 2 December 2014 / Revised: 2 February 2015 / Published online: 20 March 2015

Abstract In this paper, buckling analysis of thick functionally graded piezoelectric rectangular plates is investigated based on the higher-order shear and normal deformable plate theory. Two cases consisting of closed and open–closed circuits are considered as electrical conditions. Using the principle of minimum total potential energy and utilizing the variational approach, nonlinear governing equations for buckling analysis of thick functionally graded rectangular plates are derived. Applying the adjacent equilibrium criterion, the linear form of the governing stability equations is determined. The electric potential function is assumed to be quadratic in terms of the thickness variable. Also, it is supposed that material properties of the functionally graded plates vary through the thickness according to the power law function. Finally, the Maxwell and stability equations are solved analytically for a simply supported thick plate to obtain the critical buckling loads. Consequently, the effects of loading conditions, aspect ratio, thickness and material properties on the critical buckling loads are investigated in detail.

1 Introduction

Piezoelectric materials are materials that convert electrical current to mechanical force and vice versa. Hence, piezoelectric materials are extensively used in sensors and actuators. Because of high stress concentrations, laminated piezoelectric materials delaminate and fail. Therefore, it was proposed to fabricate a new form of piezoelectric materials with functionally graded distribution of material properties which are called functionally graded piezoelectric materials (FGPMs) [1]. In FGPMs, material properties vary continuously so that they avoid delamination and unwanted fatigue and cracks.

Plates are one of the most applicable structures in engineering which are used in different shapes. When mechanical parts are subjected to axial loads, they are deformed. For plates, the axial load is called in-plane load and acts in the middle plane of the plate. Since in-plane displacements of the plate are free, the plate buckles freely and collapses. The buckling load (in-plane load) is increased to the critical buckling load which leads to instability of plates. Since deformations in buckling are large, nonlinear equations govern the buckling. But it was shown that for pre-buckling analysis, linear equations are accurate but for the post-buckling, nonlinear forms must be used [2]. Therefore, it is important for the researchers to study the stability behavior of plates. Javaheri and Eslami [3] investigated the buckling analysis of functionally graded rectangular plates under in-plane compressive loads. The study was based on the classical plate theory, and the Navier solution was

M. Abdollahi · M. Mohammadi (✉)
Department of Mechanical Engineering, Vali-e-Asr University of Rafsanjan, Rafsanjan, Iran
E-mail: meisam.mohammadi@hotmail.com
Tel.: +98-341-2111763
Fax: +98-341-2120964

A. R. Saidi
Department of Mechanical Engineering, Shahid Bahonar University of Kerman, Kirman, Iran

presented. Buckling analysis of functionally graded rectangular plates subjected to nonlinear distributed in-plane edge loads was presented by Chen and Liew [4]. They used a mesh-free method for determining critical buckling loads. Shariat and Eslami [5] studied buckling of FG plates based on third-order shear deformation theory. It was assumed that the plate is loaded by mechanical and thermal loads and a closed form solution for the buckling loads was obtained. Oyekoya et al. [6] investigated frequencies and buckling analysis of functionally graded composite rectangular plates based on the finite element method. They applied a Mindlin-type element and a Reissner-type element for modeling the plate and concluded that the Reissner-type element gives more accurate results in comparison with the Mindlin-type element. Mirzaeifar et al. [7] presented an approximate method for simultaneous modification of natural frequencies and buckling loads. Saidi et al. [8] evaluated the bending and buckling of thick functionally graded circular plates based on third-order shear deformation plate theory. Some studies on the buckling of functionally graded rectangular plates under various loads were done by Mohammadi et al. [9,10]. The research was based on the classical and first-order shear deformation plate theories. They introduced a new method for decoupling the governing stability equations and used the Levy method for solving the equations analytically. Bodaghi and Saidi [11] developed a third-order shear deformation theory for determining the critical buckling loads of thick plates. Symmetric and asymmetric boundary conditions were considered. An accurate method for determining the critical buckling loads for thick orthotropic plates was presented by Naderi and Saidi [12]. They investigated the pre-buckling deformations and showed that pre-buckling deformations affect the critical buckling loads. The brief review offered in the literature shows that investigation of buckling of functionally graded plates with various theories is one of the most interesting subjects in engineering.

Tiersten [13] studied the basis of electromechanical characteristics for piezoelectric materials and also investigated vibrations of piezoelectric plates. Buckling of cylindrical and piezoelectric rectangular plates was carried out by Yang [14]. In the referred study, the effect of piezoelectric on the critical buckling load was shown and it was inferred that the effect of piezoelectric on the response of plates is inevitable. Krommer and Irschik [15] investigated quasi-static thermal bending, free, forced and actuated vibration of moderately thick plates with piezo-elastic layers. They focused on the existing coupling between mechanical, electrical and thermal fields with respect to the direct piezoelectric and the pyroelectric effects. The effects of shear and rotatory inertia were considered in the kinematic approximations. The effects of shape and size of piezo-ceramic actuators on the buckling load carrying capacity were expanded by Batra and Gong [16]. Shen [17] showed the post-buckling of laminated plates with piezoelectric actuators and all edges simply supported based on Reddy's higher-order shear deformation plate theory. Combinations of mechanical, electrical and thermal loads were considered, and it was assumed that material properties are independent of temperature and electric field. In another study, Shen [18] presented the thermal post-buckling analysis of FG plates with piezoelectric fiber reinforced composite actuators. Material properties were assumed to be temperature-dependent. Research was based on the third-order shear deformation theory, and simply supported boundary conditions were considered. Considering the piezoelectric eigenstrains, linear vibration of Reissner–Mindlin-type composite plates was done by Krommer [19]. It was assumed that eigenstrains are generated by applying the electrical fields to the piezoelectric layers. Boundary conditions and also electromechanically coupled fields were determined. The mechanical displacements were estimated by means of the kinematic hypothesis of Hencky. The distribution of the electric potential was obtained by superposition of a linear and a parabolic distribution in the thickness direction. The electromechanically coupled behavior was considered by the constitutive relations. It was shown that the non-local constitutive relations bring a novel concept into the theory of plates. Varelis and Saravanos [20] studied pre-buckling and post-buckling of composite plates with piezo-actuators and sensors based on the finite element method under in-plane electromechanical loading. Kapuria and Achary [21] investigated buckling of hybrid piezoelectric plates under electromechanical loads by applying nonlinear coupled zigzag theory. They obtained an analytical solution for the buckling of plates with all edges simply supported under uniaxial and biaxial strains and also the effect of electric potential. Dynamic analysis of buckling for laminated plates with piezoelectric layers under electromechanical and thermal loads was done by Shariat [22]. Also, higher-order shear deformation plate theory and finite element method were used for determining the critical loads. Buckling and free vibration analyses of piezoelectric composite plates using the spline finite strip method with higher-order shear deformation theory were studied by Akhras and Li [23]. They showed the effects of thickness, mechanical and electrical boundary conditions on the natural frequencies and critical buckling loads. Jadhav and Bajoria [24] obtained buckling of functionally graded rectangular plates with piezoelectric actuators and sensors on the upper and lower surface with all edges simply supported which is subjected to electromechanical loading. First-order shear deformation plate theory and finite element method were utilized. Khorshidvand et al. [25] studied the buckling analysis of a porous functionally graded circular plate with sensor–actuator

layers of piezoelectric. They considered uniform radial compressive loads on the clamped edges. Finally, the variation of critical buckling load versus the change of piezoelectric layers, piezoelectric layer-to-porous plate thickness ratio and feedback gain were investigated. Bodaghi and Shakeri [26] studied free vibration and transient response of functionally graded piezoelectric cylindrical panels subjected to impulsive loads based on the first-order shear deformation theory. They used both Maxwell equation and Hamilton principle and considered simply supported boundary conditions. An analytical approach for free vibration analysis of thick functionally graded rectangular plates with piezoelectric layers was presented by Askari Farsangi and Saidi [27]. First-order shear deformation plate theory was used, and Levy boundary conditions were utilized in the study.

Plate theories are not exact, and the results differ from the exact 3D elasticity solutions. Hence, it is usually important for the researchers to improve the efficiency of a theory to have accurate results in addition to simplicity of solution. Batra and Vidoli [28] for the first time used a new theory, called higher-order shear and normal deformable theory, for piezoelectric plates, which is more accurate than general plate theories, and the results are in a good agreement with the 3D elasticity solutions. According to this theory, Legendre polynomials are used to approximate the displacement field components in the thickness direction. Batra and Aimmanee [29] studied vibrations and stress distribution for isotropic rectangular plates using the higher-order shear and normal deformable plate theory. Using the principle of virtual work, vibration of incompressible plates based on the higher-order shear and normal deformable plate theory was done by Batra [30]. Sheikholeslami and Saidi [31] obtained natural frequencies for free vibration of functionally graded rectangular plates resting on elastic foundation with all edges simply supported based on the higher-order shear and normal deformable plate theory. They showed that by using higher-order theory of fifth-order, results are very close to the corresponding obtained results from 3D elasticity theory.

In this paper, higher-order shear and normal deformable plate theory is used for buckling analysis of thick functionally graded piezoelectric rectangular plates. Using a variational approach and the principle of minimum total potential energy, governing equations are obtained. Governing stability equations and also the Maxwell equation are solved analytically for a simply supported plate. Finally, the effects of dimension and material properties on the critical buckling loads are investigated.

2 Constitutive equations of functionally graded piezoelectric materials

Piezoelectric materials are smart materials that convert mechanical or electrical excitation to each other. To model the behavior of piezoelectric materials, stresses are considered as combination of mechanical and electrical fields. Thus, for a transversely piezoelectric material, the constitutive equations are

$$\begin{Bmatrix}\sigma_{11}\\ \sigma_{22}\\ \sigma_{33}\\ \sigma_{23}\\ \sigma_{13}\\ \sigma_{12}\end{Bmatrix} = \begin{bmatrix} C_{11} & C_{12} & C_{13} & 0 & 0 & 0 \\ C_{12} & C_{11} & C_{13} & 0 & 0 & 0 \\ C_{13} & C_{13} & C_{33} & 0 & 0 & 0 \\ 0 & 0 & 0 & C_{55} & 0 & 0 \\ 0 & 0 & 0 & 0 & C_{55} & 0 \\ 0 & 0 & 0 & 0 & 0 & \frac{1}{2}(C_{11}-C_{12}) \end{bmatrix} \begin{Bmatrix}\varepsilon_{11}\\ \varepsilon_{22}\\ \varepsilon_{33}\\ \gamma_{23}\\ \gamma_{13}\\ \gamma_{12}\end{Bmatrix} - \begin{bmatrix} 0 & 0 & e_{31} \\ 0 & 0 & e_{31} \\ 0 & 0 & e_{33} \\ 0 & e_{15} & 0 \\ e_{15} & 0 & 0 \\ 0 & 0 & 0 \end{bmatrix} \begin{Bmatrix}E_1\\ E_2\\ E_3\end{Bmatrix}, \tag{1a}$$

$$\begin{Bmatrix}D_1\\ D_2\\ D_3\end{Bmatrix} = \begin{bmatrix} 0 & 0 & 0 & 0 & e_{15} & 0 \\ 0 & 0 & 0 & e_{15} & 0 & 0 \\ e_{31} & e_{31} & e_{33} & 0 & 0 & 0 \end{bmatrix} \begin{Bmatrix}\varepsilon_{11}\\ \varepsilon_{22}\\ \varepsilon_{33}\\ \gamma_{23}\\ \gamma_{13}\\ \gamma_{12}\end{Bmatrix} + \begin{bmatrix} \Xi_{11} & 0 & 0 \\ 0 & \Xi_{11} & 0 \\ 0 & 0 & \Xi_{33} \end{bmatrix} \begin{Bmatrix}E_1\\ E_2\\ E_3\end{Bmatrix}, \tag{1b}$$

in which the matrix $[C]$ is the piezoelectric material stiffness matrix, $[e]$ is the electromechanical coupling matrix, $\{E\}$ and $\{D\}$ denote the electric field and electric displacement vectors, respectively, and $[\Xi]$ is the matrix of dielectric permittivity.

The electric field is related to the electric potential by the following relation [27]:

$$\vec{E} = -\vec{\nabla}\phi. \tag{2}$$

Also, it is assumed that the electric potential has a quadratic variation in the thickness direction as follows:

$$\phi(x, y, z) = A(x, y)z + B(x, y) + \left(1 - \left(\frac{2z}{h}\right)^2\right)\varphi(x, y), \tag{3}$$

where the constants A and B are determined from the electrical boundary conditions. Hence, two different cases are considered, closed and open–closed circuits. These cases are discussed in the following.

(I) Closed circuit
In closed circuit, the lower and upper surfaces of plate are connected to zero voltage. Therefore, the electrical boundary conditions for closed circuit are defined as

$$\phi\left(x, y, -\frac{h}{2}\right) = \phi\left(x, y, \frac{h}{2}\right) = 0. \tag{4}$$

By imposing the conditions (4) on the function (3), constants are obtained as

$$A = B = 0. \tag{5}$$

(II) Open–closed circuit
In open–closed circuit, it is supposed that the lower surface is connected to zero voltage and the upper surface is electrically insulated. Thus, the electrical boundary conditions for this state are

$$\phi\left(x, y, -\frac{h}{2}\right) = 0, \tag{6a}$$

$$D_z\left(x, y, \frac{h}{2}\right) = 0. \tag{6b}$$

Applying the relations (6) to Eqs. (3) and (1b) leads to

$$B(x, y) = A(x, y)\frac{h}{2}, \tag{7a}$$

$$A(x, y) = \left\{\frac{1}{\Xi_{33}}\left[e_{31}\varepsilon_{11} + e_{31}\varepsilon_{22} + e_{33}\varepsilon_{33}\right] + \frac{8z}{h^2}\varphi(x, y)\right\}_{z=\frac{h}{2}}. \tag{7b}$$

Functionally graded materials (FGMs) are new composites with special properties. In FGMs, material properties are usually considered as a function of coordinates which makes smooth variation of properties. Developing the model of functional distribution of material properties for piezoelectric materials leads to have new materials with high performance in comparison with the other materials. Hence, material properties (mechanical and electrical) in FGPMs vary through the thickness by the power law function as [9]

$$\theta(z) = \theta_1 + (\theta_2 - \theta_1)\left(\frac{1}{2} - \frac{z}{h}\right)^N, \tag{8}$$

where θ indicates a material property, N is the index of the FGPM and h is the thickness. Also, subscripts 1 and 2 show the upper ($z = h/2$) and lower ($z = -h/2$) surfaces, respectively.

3 Governing equations

Consider a rectangular plate as shown in Fig. 1 in Cartesian coordinates. The dimension h is measured in the thickness direction.

Since the considered plate is moderately thick, higher-order shear and normal deformable theory is used which is the closest theory to the 3D theory of elasticity. According to this theory, Legendre polynomials (explained in the "Appendix") are applied to approximate the displacement components in the thickness direction. Therefore, the displacement field is considered as [30]

$$u_i(x, y, z) = L_a(z)u_i^a(x, y), \quad i = 1, 2, 3. \tag{9}$$

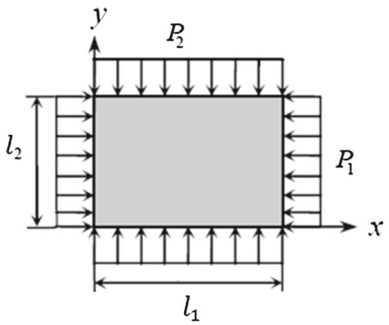

Fig. 1 Rectangular plate under compressive loads

In Eq. (9), index i refers to the coordinate and index a refers to the summation from zero to the order of theory.

Utilizing Eq. (A-4) which is prescribed in the "Appendix", derivatives of displacement components are obtained as

$$u_{i,j}(x,y,z) = L_a(z)u^a_{i,j}(x,y), \quad i = 1,2,3, \quad j = 1,2, \tag{10a}$$

$$u_{i,3}(x,y,z) = D_{ab}L_b(z)u^a_i(x,y), \quad i = 1,2,3. \tag{10b}$$

Based on the Von Karman hypothesis for nonlinear form of strain–displacement components, the strain components are determined as

$$\begin{Bmatrix} \varepsilon_{11} \\ \varepsilon_{22} \\ \varepsilon_{33} \\ \varepsilon_{12} \\ \varepsilon_{13} \\ \varepsilon_{23} \end{Bmatrix} = \begin{Bmatrix} L_a u^a_{1,1} + \frac{1}{2}L_aL_bu^a_{3,1}u^b_{3,1} \\ L_a u^a_{2,2} + \frac{1}{2}L_aL_bu^a_{3,2}u^b_{3,2} \\ D_{ab}L_bu^a_3 + \frac{1}{2}D_{ab}D_{cd}L_bL_du^a_3u^c_3 \\ \frac{1}{2}\left(L_au^a_{1,2} + L_au^a_{2,1} + L_aL_bu^a_{3,1}u^b_{3,2}\right) \\ \frac{1}{2}\left(D_{ab}L_bu^a_1 + L_au^a_{3,1} + D_{ab}L_bL_cu^a_3u^c_{3,1}\right) \\ \frac{1}{2}\left(D_{ab}L_bu^a_2 + L_au^a_{3,2} + D_{ab}L_bL_cu^a_3u^c_{3,2}\right) \end{Bmatrix}. \tag{11}$$

Using the principle of minimum total potential energy and a variational approach, the equilibrium equations are determined as

$$\delta u^a_1 : M^a_{11,1} - D_{ab}M^b_{13} + M^a_{12,2} = 0, \tag{12a}$$

$$\delta u^a_2 : M^a_{22,2} - D_{ab}M^b_{23} + M^a_{12,1} = 0, \tag{12b}$$

$$\begin{aligned} \delta u^a_3 : &- \left(M^{ab}_{11}u^b_{3,1}\right)_{,1} - \left(M^{ab}_{22}u^b_{3,2}\right)_{,2} + D_{ab}M^b_{33} + D_{ab}D_{cd}M^{bd}_{33}u^c_3 \\ &- \left(M^{ab}_{12}u^b_{3,2}\right)_{,1} - \left(M^{ab}_{12}u^b_{3,1}\right)_{,2} - M^a_{13,1} + D_{ab}M^{bc}_{13}u^c_{3,1} - D_{cb}\left(M^{ab}_{13}u^c_3\right)_{,1} - M^a_{23,2} \\ &+ D_{ab}M^{bc}_{23}u^c_{3,2} - D_{cb}\left(M^{ab}_{23}u^c_3\right)_{,2} = 0, \end{aligned} \tag{12c}$$

so that the resultant stresses are defined as

$$M^a_{ij} = \int_{-\frac{h}{2}}^{\frac{h}{2}} \sigma_{ij}L_a(z)\mathrm{d}z, \qquad i,j = 1,2,3, \tag{13a}$$

$$M^{ab}_{ij} = \int_{-\frac{h}{2}}^{\frac{h}{2}} \sigma_{ij}L_a(z)L_b(z)\mathrm{d}z, \qquad i,j = 1,2,3. \tag{13b}$$

In addition, the boundary conditions are obtained as

$$\delta u_1^a = 0 \quad \text{or } M_{11}^a \mathbf{e}_1 + M_{12}^a \mathbf{e}_2 + P_1 L_a(0)\mathbf{e}_1 = 0, \tag{14a}$$
$$\delta u_2^a = 0 \quad \text{or } M_{22}^a \mathbf{e}_2 + M_{12}^a \mathbf{e}_1 + P_2 L_a(0)\mathbf{e}_2 = 0, \tag{14b}$$
$$\delta u_3^a = 0 \quad \text{or } M_{11}^{ab} u_{3,1}^b \mathbf{e}_1 + M_{22}^{ab} u_{3,2}^b \mathbf{e}_2 + M_{12}^{ab} u_{3,2}^b \mathbf{e}_1 + M_{12}^{ab} u_{3,1}^b \mathbf{e}_2 + M_{13}^a \mathbf{e}_1 + D_{cb} M_{13}^{ab} u_3^c \mathbf{e}_1 + M_{23}^a \mathbf{e}_2 + D_{cb} M_{23}^{ab} u_3^c \mathbf{e}_2 = 0. \tag{14c}$$

In Eq. (14), P_1 and P_2 are the external in-plane loads on the edges. Since the strain components are nonlinear in terms of displacement components, the stresses and resultant stresses are nonlinear, too. In order to study the pre-buckling of plate, linear forms of governing equations are needed. Hence, the adjacent equilibrium criterion is used to obtain the linear forms of the governing equations. Based on this criterion, a plate is stable if the displacement components vary incrementally from the equilibrium state. Therefore, two states are considered, equilibrium state (with nonlinear form of governing equations) and neighboring state (with linear form of governing equations) [9]. In the following, the superscripts $(-)$ and $(\sim)$ refer to the equilibrium and neighboring states, respectively. So, the displacement components are written as

$$u_i^a = \bar{u}_i^a + \tilde{u}_i^a. \tag{15}$$

Consequently, the resultant stresses are expressed in the following form:

$$M_{ij}^a = \bar{M}_{ij}^a + \tilde{M}_{ij}^a, \tag{16a}$$
$$M_{ij}^{ab} = \bar{M}_{ij}^{ab} + \tilde{M}_{ij}^{ab}. \tag{16b}$$

By substituting the new forms of (16) in the equilibrium equations (12), stability equations which are linear form of equilibrium equations are determined so that

$$\delta u_1^a : \tilde{M}_{11,1}^a - D_{ab}\tilde{M}_{13}^b + \tilde{M}_{12,2}^a = 0, \tag{17a}$$
$$\delta u_2^a : \tilde{M}_{22,2}^a - D_{ab}\tilde{M}_{23}^b + \tilde{M}_{12,1}^a = 0, \tag{17b}$$
$$\delta u_3^a : -\bar{M}_{11}^{ab}\tilde{u}_{3,11}^b - \bar{M}_{22}^{ab}\tilde{u}_{3,22}^b + D_{ab}\tilde{M}_{33}^b - \tilde{M}_{13,1}^a - \tilde{M}_{23,2}^a = 0. \tag{17c}$$

It must be noted that in the above stability equations, equilibrium equations are satisfied. Also, terms with superscript $(-)$ indicate the pre-buckling forces which are determined from the equilibrium conditions.

Applying the adjacent equilibrium criterion to the boundary conditions leads to

$$\delta\tilde{u}_1^a = 0 \quad \text{or } \tilde{M}_{11}^a \mathbf{e}_1 + \tilde{M}_{12}^a \mathbf{e}_2 = 0, \tag{18a}$$
$$\delta\tilde{u}_2^a = 0 \quad \text{or } \tilde{M}_{22}^a \mathbf{e}_2 + \tilde{M}_{12}^a \mathbf{e}_1 = 0, \tag{18b}$$
$$\delta\tilde{u}_3^a = 0 \quad \text{or } \bar{M}_{11}^{ab}\tilde{u}_{3,1}^b \mathbf{e}_1 + \bar{M}_{22}^{ab}\tilde{u}_{3,2}^b \mathbf{e}_2 + \tilde{M}_{13}^a \mathbf{e}_1 + \tilde{M}_{23}^a \mathbf{e}_2 = 0. \tag{18c}$$

Upon substituting the resultant stresses in terms of strains and displacements, the governing stability equations are determined as

$$\int_{-\frac{h}{2}}^{\frac{h}{2}} \Big[L_a L_c C_{11}\tilde{u}_{1,11}^c + L_a L_c C_{12}\tilde{u}_{2,21}^c + D_{cd} L_a L_d C_{13}\tilde{u}_{3,1}^c + L_a e_{31}\tilde{\phi}_{,31} - D_{ab}\left(D_{cd} L_b L_d C_{55}\tilde{u}_1^c + L_b L_c C_{55}\tilde{u}_{3,1}^c + L_b e_{15}\tilde{\phi}_{,1}\right) + \frac{1}{2} L_a L_c (C_{11} - C_{12})\tilde{u}_{1,22}^c + \frac{1}{2} L_a L_c (C_{11} - C_{12})\tilde{u}_{2,12}^c \Big] \mathrm{d}z = 0, \tag{19a}$$

$$\int_{-\frac{h}{2}}^{\frac{h}{2}}\Big[L_aL_cC_{12}\tilde{u}^c_{1,12}+L_aL_cC_{11}\tilde{u}^c_{2,22}+D_{cd}L_aL_dC_{13}\tilde{u}^c_{3,2}+L_ae_{31}\tilde{\phi}_{,32}$$
$$-D_{ab}\left(D_{cd}L_bL_dC_{55}\tilde{u}^c_2+L_bL_cC_{55}\tilde{u}^c_{3,2}+L_be_{15}\tilde{\phi}_{,2}\right)$$
$$+\frac{1}{2}L_aL_c(C_{11}-C_{12})\tilde{u}^c_{1,21}+\frac{1}{2}L_aL_c(C_{11}-C_{12})\tilde{u}^c_{2,11}\Big]\mathrm{d}z=0, \tag{19b}$$

$$\int_{-\frac{h}{2}}^{\frac{h}{2}}\Big[D_{ab}\left(L_bL_cC_{13}\tilde{u}^c_{1,1}+L_bL_cC_{13}\tilde{u}^c_{2,2}+D_{cd}L_bL_dC_{33}\tilde{u}^c_3+L_be_{33}\tilde{\phi}_{,3}\right)$$
$$-D_{cd}L_aL_dC_{55}\tilde{u}^c_{1,1}-L_aL_cC_{55}\tilde{u}^c_{3,11}-L_ae_{15}\tilde{\phi}_{,11}-D_{cd}L_aL_dC_{55}\tilde{u}^c_{2,2}$$
$$-L_aL_cC_{55}\tilde{u}^c_{3,22}-L_ae_{15}\tilde{\phi}_{,22}\Big]\mathrm{d}z-\bar{M}^{ac}_{11}\tilde{u}^c_{3,11}-\bar{M}^{ac}_{22}\tilde{u}^c_{3,22}=0. \tag{19c}$$

To satisfy the electrical conditions, the appropriate Maxwell equation must be dealt with. Thus,

$$\int_{-\frac{h}{2}}^{\frac{h}{2}}\vec{\nabla}\cdot\vec{D}\mathrm{d}z=\int_{-\frac{h}{2}}^{\frac{h}{2}}(D_{1,1}+D_{2,2}+D_{3,3})\mathrm{d}z=0. \tag{20}$$

Replacing Eq. (1b) in the Maxwell equation and simplifying the results lead to

$$\int_{-\frac{h}{2}}^{\frac{h}{2}}\Big[e_{15}\gamma_{13,1}+\Xi_{11}E_{1,1}+e_{15}\gamma_{23,2}+\Xi_{11}E_{2,2}+e_{31,3}\varepsilon_{11}+e_{31}\varepsilon_{11,3}+e_{31,3}\varepsilon_{22}+e_{31}\varepsilon_{22,3}$$
$$+e_{33,3}\varepsilon_{33}+e_{33}\varepsilon_{33,3}+\Xi_{33,3}E_3+\Xi_{33}E_{3,3}\Big]\mathrm{d}z=0. \tag{21}$$

Using the strains presented in Eq. (11), Eq. (21) is simplified as

$$\int_{-\frac{h}{2}}^{\frac{h}{2}}\Big[e_{15}\left(D_{cd}L_d\tilde{u}^c_{1,1}+L_c\tilde{u}^c_{3,11}\right)-\Xi_{11}\tilde{\phi}_{,11}+e_{15}\left(D_{cd}L_d\tilde{u}^c_{2,2}+L_c\tilde{u}^c_{3,22}\right)$$
$$-\Xi_{11}\tilde{\phi}_{,22}+e_{31,3}L_c\tilde{u}^c_{1,1}+e_{31}D_{cd}L_d\tilde{u}^c_{1,1}$$
$$+e_{31,3}L_c\tilde{u}^c_{2,2}+e_{31}D_{cd}L_d\tilde{u}^c_{2,2}+e_{33,3}D_{cd}L_d\tilde{u}^c_3$$
$$+e_{33}D_{cd}D_{df}L_f\tilde{u}^c_3-\Xi_{33,3}\tilde{\phi}_{,3}-\Xi_{33}\tilde{\phi}_{,33}\Big]\mathrm{d}z=0. \tag{22}$$

In the stability and Maxwell equations, the function $\tilde{\phi}$ is the electric potential in the neighboring state. Thus, applying the adjacent equilibrium criterion results in

$$\tilde{\phi}=\tilde{A}(x,y)z+\tilde{B}(x,y)+\left(1-\left(\frac{2z}{h}\right)^2\right)\tilde{\varphi}(x,y). \tag{23}$$

4 Boundary conditions

For solving the stability and Maxwell equations, boundary conditions are needed. Let the plate be simply supported on all the edges. Using the variational approach and divergence theorem, the following boundary conditions are determined:

$$\tilde{u}^a_3=\tilde{M}^a_{11}=\tilde{M}^a_{12}=0\quad\text{on } x=0,l_1, \tag{24a}$$
$$\tilde{u}^a_3=\tilde{M}^a_{22}=\tilde{M}^a_{12}=0\quad\text{on } y=0,l_2. \tag{24b}$$

Also by applying the adjacent equilibrium criterion, the constants in Eqs. (5) and (7) are simplified as

(I) Closed circuit

$$\tilde{A}=\tilde{B}=0 \tag{25}$$

(II) Open-closed circuit

$$\tilde{B}(x,y) = \tilde{A}(x,y)\frac{h}{2}, \tag{26a}$$

$$\tilde{A}(x,y) = \frac{1}{\Xi_{33}\left(\frac{h}{2}\right)}\left[e_{31}\left(\frac{h}{2}\right)L_c\left(\frac{h}{2}\right)\tilde{u}^c_{1,1} + e_{31}\left(\frac{h}{2}\right)L_c\left(\frac{h}{2}\right)\tilde{u}^c_{2,2} + e_{33}\left(\frac{h}{2}\right)D_{cd}L_d\left(\frac{h}{2}\right)\tilde{u}^c_3\right] + \frac{4}{h}\tilde{\varphi}(x,y). \tag{26b}$$

To have an analytical solution, the Navier method is applied. According to this method, the unknown functions are assumed as

$$\tilde{u}^c_1 = \sum_{m=0}^{\infty}\sum_{n=0}^{\infty}\tilde{u}^{cmn}_1\cos\left(\frac{m\pi x}{l_1}\right)\sin\left(\frac{n\pi y}{l_2}\right), \tag{27a}$$

$$\tilde{u}^c_2 = \sum_{m=0}^{\infty}\sum_{n=0}^{\infty}\tilde{u}^{cmn}_2\sin\left(\frac{m\pi x}{l_1}\right)\cos\left(\frac{n\pi y}{l_2}\right), \tag{27b}$$

$$\tilde{u}^c_3 = \sum_{m=0}^{\infty}\sum_{n=0}^{\infty}\tilde{u}^{cmn}_3\sin\left(\frac{m\pi x}{l_1}\right)\sin\left(\frac{n\pi y}{l_2}\right), \tag{27c}$$

$$\tilde{\varphi} = \sum_{m=0}^{\infty}\sum_{n=0}^{\infty}\tilde{\varphi}^{mn}\sin\left(\frac{m\pi x}{l_1}\right)\sin\left(\frac{n\pi y}{l_2}\right). \tag{27d}$$

It is easy to show that the above relations satisfy the governing and Maxwell equations. Also, the boundary conditions are satisfied, exactly. To solve the stability equations, pre-buckling forces are needed which are determined from the equilibrium equations. Hence, the pre-buckling forces are obtained as

$$P_1 = -P, \tag{28a}$$

$$P_2 = RP_1 = -RP, \tag{28b}$$

where R is the loading parameter and indicates loading conditions. The plate is loaded uniaxially with compressive load for $R = 0$, biaxially and compressively while $R = 1$. Also, $R = -1$ corresponds to the combination of tensile and compressive loads.

5 Validation

In order to investigate the accuracy of the presented results, a validation is done between the obtained results and the results shown by Bodaghi and Saidi [11]. The referred study is a buckling analysis of functionally graded plates based on the third-order shear deformation plate theory (TSDT). In Table 1, critical buckling

Table 1 Comparison of the critical buckling loads

N	R	l_1/l_2	Ref. [11]	Presented study	Error (%)
0	1	1	$718.692^{(1)}$	$715.808^{(1)}$	0.403
		1.5	$526.861^{(1)}$	$525.308^{(1)}$	0.296
	0	1	$1437.361^{(1)}$	$1431.594^{(1)}$	0.403
		1.5	$1527.903^{(2)}$	$1519.588^{(2)}$	0.547
	−1	1	$2772.980^{(2)}$	$2746.842^{(2)}$	0.952
		1.5	$2772.980^{(3)}$	$2746.842^{(3)}$	0.952
1	1	1	$351.124^{(1)}$	$350.034^{(1)}$	0.311
		1.5	$256.776^{(1)}$	$256.194^{(1)}$	0.227
	0	1	$702.304^{(1)}$	$700.068^{(1)}$	0.319
		1.5	$748.920^{(2)}$	$745.801^{(2)}$	0.418
	−1	1	$1371.653^{(2)}$	$1361.174^{(2)}$	0.770
		1.5	$1371.653^{(3)}$	$1361.174^{(3)}$	0.770

Numbers in parentheses show the mode number

Table 2 Material properties of FGPM

Elastic constants									
Material	C_{11}/C^*	C_{12}/C^*	C_{13}/C^*	C_{22}/C^*	C_{23}/C^*	C_{33}/C^*	C_{44}/C^*	C_{55}/C^*	C_{66}/C^*
PZT-4	1	0.55971	0.53237	1	0.53237	0.82734	0.18417	0.18417	0.22014
PZT-5*H*	0.90647	0.56906	0.60360	0.90647	0.60360	0.84173	0.16547	0.16547	0.16906
	Piezoelectric moduli ($\mathrm{C\,m^{-2}}$)					Dielectric moduli ($10^{-9}\times \mathrm{F\,m^{-1}}$)			
	e_{15}	e_{24}	e_{31}	e_{32}	e_{33}	Ξ_{11}	Ξ_{22}	Ξ_{33}	
PZT-4	12.7	12.7	−5.2	−5.2	15.1	6.46	6.46	5.62	
PZT-5*H*	17	17	−6.5	−6.5	23.3	15.05	15.05	13.02	

Table 3 Investigation of convergence of non-dimensional results for square plate with linear distribution of material properties ($R = 0$)

h/l_2	$k=1$	$k=2$	$k=3$	$k=4$	$k=5$
Closed circuit					
0.1	$2.98101^{(1)}$	$2.40446^{(1)}$	$2.38511^{(1)}$	$2.38540^{(1)}$	$2.38288^{(1)}$
0.2	$2.46321^{(1)}$	$2.08316^{(1)}$	$2.03065^{(1)}$	$2.02479^{(1)}$	$2.02242^{(1)}$
Open-closed circuit					
0.1	$2.99266^{(1)}$	$2.42273^{(1)}$	$2.40396^{(1)}$	$2.40122^{(1)}$	$2.40165^{(1)}$
0.2	$2.52980^{(1)}$	$2.12356^{(1)}$	$2.07006^{(1)}$	$2.06019^{(1)}$	$2.06147^{(1)}$

Numbers in parentheses show the mode number

loads are compared for different power index, loading conditions and dimensions. As the table shows, there is a good agreement between the presented solution and results in Ref. [11]. There is a slight difference between the results, this is because in TSDT normal strains are neglected, but in the used theory, all strain components are encountered and the plane stress hypothesis is not used.

6 Results and discussion

In order to study the buckling loads, it is assumed that the functionally graded piezoelectric plate is made of PZT-4 ($z=-h/2$) and PZT-5*H* ($z=h/2$) with the mechanical and electrical properties as tabulated in Table 2 [26]. It must be noted that when the index of the FGPM is equal to zero, it represents an isotropic piezoelectric plate with PZT-4 material properties.

To keep the generality and simplicity, dimensionless critical buckling loads are presented in the following. Let the non-dimensional critical buckling load parameter be defined as

$$P^* = \frac{P l_2^2}{C^* h^3}, \tag{29}$$

where l_2 is the width of the plate, h is the thickness, P is the critical buckling load and $C^* = C_{11,\text{PZT-4}}$ is the elastic constant for PZT-4 which is $139\,\mathrm{GN/m^2}$.

In Table 3, non-dimensional critical buckling loads are tabulated for various orders of shear and normal deformable theories. Two cases are considered, closed and open-closed circuits. Investigation shows that results converge for the order of $k = 5$.

In Table 4, non-dimensional critical buckling loads are presented for closed and open–closed circuits. Different loading conditions and power index are considered. The table shows that for $R = 1$, increasing the aspect ratio (l_1/l_2) decreases the non-dimensional critical buckling load. Also, increasing the thickness–width ratio (h/l_2) decreases the non-dimensional critical buckling load. In addition, the non-dimensional critical buckling load has a maximum for the case of $R = -1$. According to the results shown in Table 4, the non-dimensional critical buckling load is higher for the open–closed circuit in comparison with the closed circuit. This variation is more apparent for thicker plates. As Table 4 indicates, increasing the index of the FGM decreases the non-dimensional critical buckling load.

To show the effect of piezoelectric materials on the non-dimensional critical buckling loads, a comparison is done in Table 5. Two cases are considered for the closed circuit, functionally graded (FG) plate and functionally

Table 4 Non-dimensional critical buckling loads for closed and open–closed circuits

N	l_1/l_2	h/l_2	Closed circuit			Open-closed circuit		
			$R=1$	$R=0$	$R=-1$	$R=1$	$R=0$	$R=-1$
0	0.5	0.1	$3.05511^{(1)}$	$3.81885^{(1)}$	$5.09180^{(1)}$	$3.06504^{(1)}$	$3.83122^{(1)}$	$5.10835^{(1)}$
		0.2	$2.16634^{(1)}$	$2.70793^{(1)}$	$3.61058^{(1)}$	$2.20685^{(1)}$	$2.75856^{(1)}$	$3.67809^{(1)}$
	1	0.1	$1.33683^{(1)}$	$2.67367^{(1)}$	$5.09180^{(2)}$	$1.33777^{(1)}$	$2.67547^{(1)}$	$5.10835^{(2)}$
		0.2	$1.12696^{(1)}$	$2.25391^{(1)}$	$3.61058^{(2)}$	$1.13437^{(1)}$	$2.26873^{(1)}$	$3.67809^{(2)}$
	1.5	0.1	$0.98281^{(1)}$	$2.83165^{(2)}$	$5.09180^{(3)}$	$0.98317^{(1)}$	$2.83511^{(2)}$	$5.10835^{(3)}$
		0.2	$0.86357^{(1)}$	$2.26576^{(2)}$	$3.61058^{(3)}$	$0.86709^{(1)}$	$2.28872^{(2)}$	$3.67809^{(3)}$
1	0.5	0.1	$2.73338^{(1)}$	$3.41669^{(1)}$	$4.55561^{(1)}$	$2.77165^{(1)}$	$3.46453^{(1)}$	$4.61935^{(1)}$
		0.2	$1.95581^{(1)}$	$2.44476^{(1)}$	$3.25968^{(1)}$	$2.01841^{(1)}$	$2.52301^{(1)}$	$3.36402^{(1)}$
	1	0.1	$1.19144^{(1)}$	$2.38288^{(1)}$	$4.55561^{(2)}$	$1.20086^{(1)}$	$2.40165^{(1)}$	$4.61935^{(2)}$
		0.2	$1.01122^{(1)}$	$2.02242^{(1)}$	$3.25968^{(2)}$	$1.03073^{(1)}$	$2.06147^{(1)}$	$3.36402^{(2)}$
	1.5	0.1	$0.87518^{(1)}$	$2.52655^{(2)}$	$4.55561^{(3)}$	$0.88101^{(1)}$	$2.55058^{(2)}$	$4.61935^{(3)}$
		0.2	$0.77327^{(1)}$	$2.03767^{(2)}$	$3.25968^{(3)}$	$0.78524^{(1)}$	$2.08622^{(2)}$	$3.36402^{(3)}$
2	0.5	0.1	$2.70727^{(1)}$	$3.38403^{(1)}$	$4.51209^{(1)}$	$2.74302^{(1)}$	$3.42885^{(1)}$	$4.57173^{(1)}$
		0.2	$1.94527^{(1)}$	$2.43159^{(1)}$	$3.24212^{(1)}$	$2.00010^{(1)}$	$2.50013^{(1)}$	$3.33350^{(1)}$
	1	0.1	$1.17835^{(1)}$	$2.35669^{(1)}$	$4.51209^{(2)}$	$1.18741^{(1)}$	$2.37475^{(1)}$	$4.57173^{(2)}$
		0.2	$1.00276^{(1)}$	$2.00551^{(1)}$	$3.24212^{(2)}$	$1.02068^{(1)}$	$2.04137^{(1)}$	$3.33350^{(2)}$
	1.5	0.1	$0.86525^{(1)}$	$2.49971^{(2)}$	$4.51209^{(3)}$	$0.87094^{(1)}$	$2.52273^{(2)}$	$4.57173^{(3)}$
		0.2	$0.76614^{(1)}$	$2.02270^{(2)}$	$3.24212^{(3)}$	$0.77727^{(1)}$	$2.06663^{(2)}$	$3.33350^{(3)}$

Numbers in parentheses show the mode number

Table 5 Comparison of non-dimensional critical buckling loads for FG and FGP square plates (closed circuit)

N	h/l_2	$R=1$		$R=0$		$R=-1$	
		FG plate	FGP plate	FG plate	FGP plate	FG plate	FGP plate
0	0.1	$1.00432^{(1)}$	$1.33683^{(1)}$	$2.00863^{(1)}$	$2.67367^{(1)}$	$3.78050^{(2)}$	$5.09180^{(2)}$
	0.2	$0.82748^{(1)}$	$1.12696^{(1)}$	$1.65496^{(1)}$	$2.25391^{(1)}$	$2.55058^{(2)}$	$3.61058^{(2)}$
1	0.1	$0.86245^{(1)}$	$1.19144^{(1)}$	$1.72489^{(1)}$	$2.38288^{(1)}$	$3.27259^{(2)}$	$4.55561^{(2)}$
	0.2	$0.72105^{(1)}$	$1.01122^{(1)}$	$1.44210^{(1)}$	$2.02242^{(1)}$	$2.26284^{(2)}$	$3.25968^{(2)}$

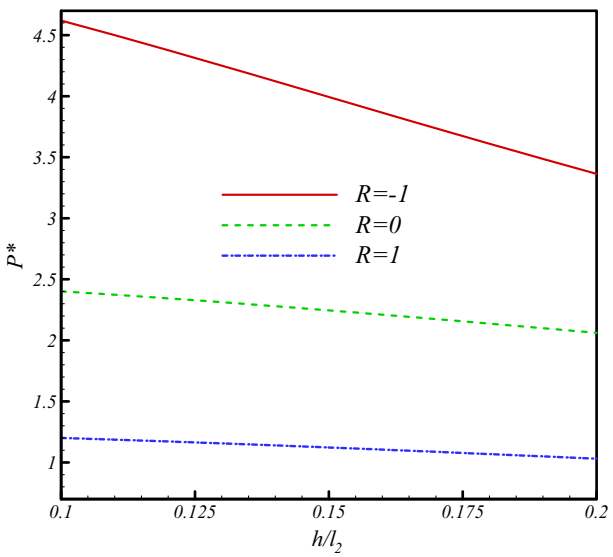

Fig. 2 Variation of non-dimensional critical buckling load versus the thickness–width ratio for square FGP plate (open–closed circuit)

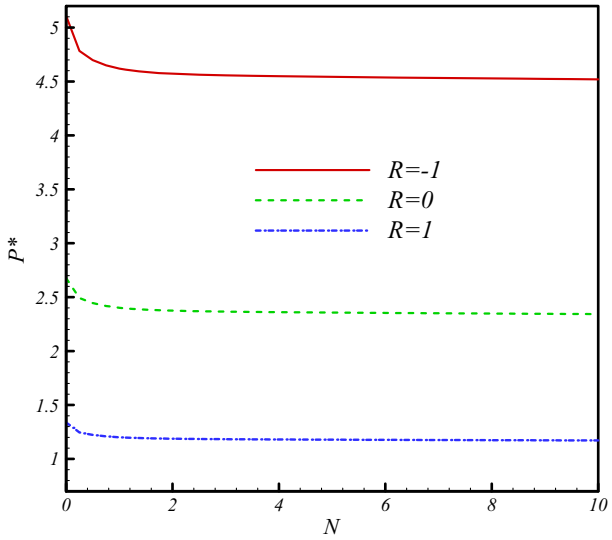

Fig. 3 Variation of non-dimensional critical buckling load with respect to the power index (open–closed circuit)

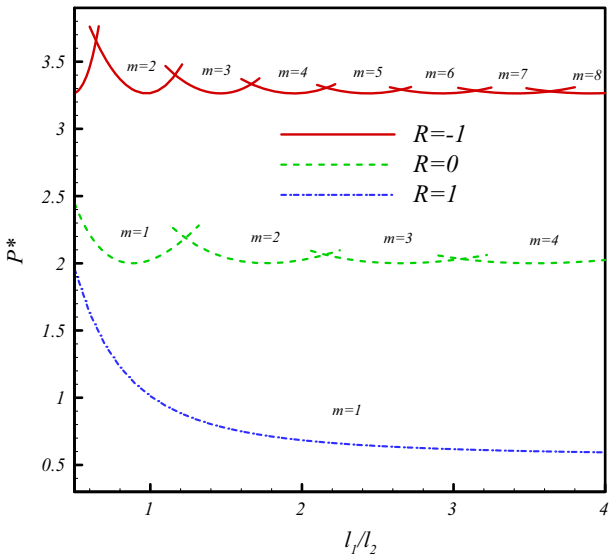

Fig. 4 Variation of mode numbers versus the aspect ratio (closed circuit)

graded piezoelectric (FGP) plate. The comparison shows that considering the piezoelectric effect increases the non-dimensional critical buckling load.

In Fig. 2, variation of non-dimensional critical buckling load versus the thickness–width ratio is depicted. Three types of loading conditions are considered. It is assumed that material properties vary linearly through the thickness. As the figure shows, increasing the thickness–width ratio decreases the non-dimensional critical buckling load. Also, the load carrying capacity is at a maximum for the case of $R = -1$.

The effect of the power index on the non-dimensional critical buckling load for a square plate is plotted in Fig. 3. It is clear that variation of the non-dimensional critical buckling load versus the index of the FGPM is more apparent for lower values of N. Also, the non-dimensional critical buckling load decreases by increasing the index of the FGPM because the flexural rigidity decreases.

In Fig. 4, the effect of aspect ratio on the mode numbers is shown. It is supposed that material properties vary linearly. As the figure shows, depending on the loading conditions buckling may occur in higher modes when the aspect ratio increases.

In Figs. 5 and 6, the variation of the non-dimensional critical buckling load with respect to the electrical condition is investigated. In Fig. 5, two cases are considered, FG plate and FGP plate. It is inferred that the

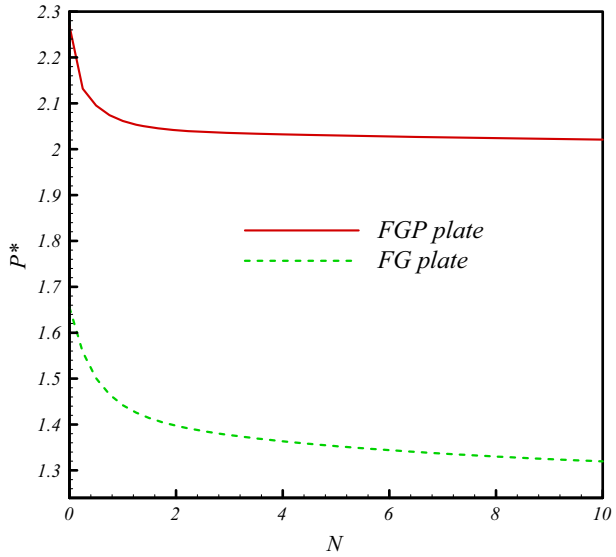

Fig. 5 Comparisons of non-dimensional critical buckling load for FG and FGP square plate in uniaxial loading (open–closed circuit)

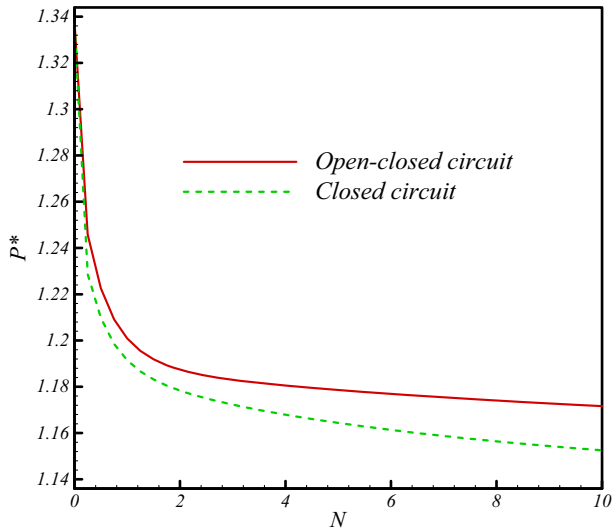

Fig. 6 Effect of non-dimensional electrical conditions on the critical buckling load versus the power index for square plate

non-dimensional critical buckling load is higher for the FGP plate in comparison with the FG plate. Therefore, the piezoelectric effect increases the flexural rigidity of the plate. Also, in Fig. 6, the non-dimensional critical buckling load for closed and open–closed circuits is plotted. It is clear that differences are more apparent when the index of the FGPM increases.

7 Conclusion

In this paper, based on the higher-order shear and normal deformable theory, buckling analysis of thick rectangular plates made of functionally graded piezoelectric materials is investigated. Two types of electrical conditions are considered, closed and open–closed circuits. Using the variational approach and the adjacent equilibrium criterion, the stability equations were determined and solved analytically for a simply supported plate. Finally, the non-dimensional critical buckling loads are determined. It is concluded that the non-dimensional critical buckling load decreases by increasing the thickness and decreases by increasing the index of the FGPM.

Also, considering piezoelectric effect increases the flexural rigidity of plate and hence the non-dimensional critical buckling load increases. Depending on the loading conditions, buckling may occur in higher modes by increasing the aspect ratio.

Appendix: Legendre polynomials

The Legendre polynomials in the z direction are defined as [31]

$$L_{n-1}(z) = \sqrt{\frac{(2n-1)}{h}} P_{n-1}(z), \qquad n \geq 1, \tag{A-1}$$

so that

$$P_0(z) = 1, \tag{A-2a}$$

$$P_1(z) = \frac{2z}{h}, \tag{A-2b}$$

$$P_{n+1}(z) = \left(\frac{2n+1}{n+1}\right)\left(\frac{2z}{h}\right) P_n(z) - \left(\frac{n}{n+1}\right) P_{n-1}(z), \tag{A-2c}$$

where n is the order of the polynomials. Legendre polynomials are orthogonal functions so that

$$\int_{-\frac{h}{2}}^{\frac{h}{2}} L_a(z) L_b(z) \mathrm{d}z = \delta_{ab}, \quad a, b = 0, 1, 2, \ldots, k. \tag{A-3}$$

In Eq. (A-3), δ is the Kronecker delta. Further, Legendre polynomial derivatives are defined as

$$L'_a(z) = D_{ab} L_b(z), \tag{A-4}$$

where D is the matrix of derivatives and for the case of $k = 5$ is determined as

$$D = \begin{bmatrix} 0 & 0 & 0 & 0 & 0 & 0 \\ \sqrt{3} & 0 & 0 & 0 & 0 & 0 \\ 0 & \sqrt{15} & 0 & 0 & 0 & 0 \\ \sqrt{7} & 0 & \sqrt{35} & 0 & 0 & 0 \\ 0 & 3\sqrt{3} & 0 & 3\sqrt{7} & 0 & 0 \\ \sqrt{11} & 0 & \sqrt{55} & 0 & 3\sqrt{11} & 0 \end{bmatrix}. \tag{A-5}$$

The matrix D for other values of k is available in Refs. [28,30].

References

1. Jam, J.E., Nia, N.G.: Dynamic analysis of FGPM annular plate based on the 3-D theory of elasticity. Int. J. Compos. Mater. **2**, 53–62 (2012)
2. Brush, D.O., Almroth, B.O.: Buckling of Bars, Plates and Shells. McGraw-Hill, New York (1975)
3. Javaheri, R., Eslami, M.R.: Buckling of functionally graded rectangular plates under in plane compressive loading. ZAMM **82**, 277–283 (2002)
4. Chen, X.L., Liew, K.M.: Buckling of rectangular functionally graded materials plates subjected to nonlinearly distributed in-plane edge loads. Smart Mater. Struct. **13**, 1430–1437 (2004)
5. Shariat, B.A.S., Eslami, M.R.: Buckling of thick functionally graded plates under mechanical and thermal loads. Compos. Struct. **78**, 433–439 (2007)
6. Oyekoya, O.O., Mba, D.U., El-Zafrany, A.M.: Buckling and vibration analysis of functionally graded composite structures using the finite element method. Compos. Struct. **89**, 134–142 (2009)
7. Mirzaeifar, R., Shahaba, S., Bahai, H.: An approximate method for simultaneous modification of natural frequencies and buckling loads of thin rectangular isotropic plates. Eng. Struct. **31**, 208–215 (2009)
8. Saidi, A.R., Rasouli, A., Sahraee, S.: Axisymmetric bending and buckling analysis of thick functionally graded circular plates using unconstrained third-order shear deformation plate theory. Compos. Struct. **89**, 110–119 (2009)
9. Mohammadi, M., Saidi, A.R., Jomehzadeh, E.: A novel analytical approach for the buckling analysis of moderately thick functionally graded rectangular plates with two simply-supported opposite edges. Mech. Eng. Sci. **224**, 1831–1841 (2010)

10. Mohammadi, M., Saidi, A.R., Jomehzadeh, E.: Levy solution for buckling analysis of functionally graded rectangular plates. Appl. Compos. Mater. **17**, 81–93 (2010)
11. Bodaghi, M., Saidi, A.R.: Levy-type solution for buckling analysis of thick functionally graded rectangular plates based on the higher-order shear deformation plate theory. Appl. Math. Model. **34**, 3659–3673 (2010)
12. Naderi, A., Saidi, A.R.: On pre-buckling configuration of functionally graded Mindlin rectangular plates. Mech. Res. Commun. **37**, 535–538 (2010)
13. Tiersten, H.F.: Linear Piezoelectric Plate Vibration. Plenum Press, New York (1969)
14. Yang, J.S.: Buckling of a piezoelectric plate. J. Appl. Electromagn. Mech. **9**, 399–408 (1998)
15. Krommer, M., Irschik, H.: A Reissner–Mindlin-type plate theory including the direct piezoelectric and the pyroelectric effect. Acta Mech. **141**, 51–69 (2000)
16. Batra, R.C., Geng, T.S.: Enhancement of the dynamic buckling load for a plate by using piezoceramic actuators. Smart Mater. Struct. **10**, 925–933 (2001)
17. Shen, H.S.: Postbuckling of shear deformable laminated plates with piezoelectric actuators under complex loading conditions. Int. J. Solids Struct. **38**, 7703–7721 (2001)
18. Shen, H.S.: A comparison of buckling and postbuckling behavior of FGM plates with piezoelectric fiber reinforced composite actuators. Compos. Struct. **91**, 375–384 (2009)
19. Krommer, M.: Piezoelastic vibrations of composite Reissner–Mindlin-type plates. J. Sound Vib. **263**, 871–891 (2003)
20. Varelis, D., Saravanos, D.A.: Coupled buckling and postbuckling analysis of active laminated piezoelectric composite plates. Int. J. Solids Struct. **41**, 1519–1538 (2004)
21. Kapuria, S., Achary, G.G.S.: Nonlinear coupled zigzag theory for buckling of hybrid piezoelectric plates. Compos. Struct. **74**, 253–264 (2006)
22. Shariyat, M.: Dynamic buckling of imperfect laminated plates with piezoelectric sensors and actuators subjected to thermo-electro-mechanical loadings, considering the temperature dependency of the material properties. Compos. Struct. **88**, 228–239 (2009)
23. Akhras, G., Li, W.: Stability and free vibration analysis of thick piezoelectric composite plates using spline finite strip method. Int. J. Mech. Sci. **53**, 575–584 (2011)
24. Jadhav, P., Bajoria, K.: Stability analysis of piezoelectric FGM plate subjected to electro-mechanical loading using finite element method. Int. J. Appl. Sci. Eng. **11**, 375–391 (2013)
25. Khorshidvand, A.R., Farzaneh Joubaneh, E., Jabbari, M., Eslami, M.R.: Buckling analysis of a porous circular plate with piezoelectric sensor–actuator layers under uniform radial compression. Acta Mech. **225**, 179–193 (2014)
26. Bodaghi, M., Shakeri, M.: An analytical approach for free vibration and transient response of functionally graded piezoelectric cylindrical panels subjected to impulsive loads. Compos. Struct. **94**, 1721–1735 (2012)
27. Askari Farsangi, M.A., Saidi, A.R.: Levy type solution for free vibration analysis of functionally graded rectangular plates with piezoelectric layers. Smart Mater. Struct. **21**, 1–15 (2012)
28. Batra, R.C., Vidoli, S.: Higher order piezoelectric plate theory derived from a three-dimensional variational principle. AIAA J. **40**, 91–104 (2002)
29. Batra, R.C., Aimmanee, S.: Vibrations of thick isotropic plates with higher order shear and normal deformable plate theories. Comput. Struct. **83**, 934–955 (2005)
30. Batra, R.C.: Higher-order shear and normal deformable theory for functionally graded incompressible linear elastic plates. Thin-Walled Struct. **45**, 974–982 (2007)
31. Sheikholeslami, S.A., Saidi, A.R.: Vibration analysis of functionally graded rectangular plates resting on elastic foundation using higher-order shear and normal deformable plate theory. Compos. Struct. **106**, 350–361 (2013)